



## The Lantern: An ultra-light micro-drive for multi-tetrode recordings in mice and other small animals

Francesco P. Battaglia<sup>a</sup>, Tobias Kalenscher<sup>a</sup>, Henrique Cabral<sup>a</sup>, Jasper Winkel<sup>a</sup>, Jeroen Bos<sup>a</sup>, Ron Manuputy<sup>b</sup>, Theo van Lieshout<sup>b</sup>, Frans Pinkse<sup>b</sup>, Harry Beukers<sup>b</sup>, Cyriel Pennartz<sup>a,\*</sup>

<sup>a</sup> Center for Neuroscience, Swammerdam Institute for Life Sciences, Faculty of Science, Universiteit van Amsterdam, P.O. box 94084, Kruislaan 320, 1090GB Amsterdam, The Netherlands

<sup>b</sup> Department of Technology, Faculty of Science, Universiteit van Amsterdam, The Netherlands

### ARTICLE INFO

#### Article history:

Received 15 September 2008

Received in revised form 11 December 2008

Accepted 17 December 2008

#### Keywords:

Ensemble electrophysiology

Mouse

Miniaturization

Tetrodes

### ABSTRACT

*In vivo* electrophysiological recordings from groups of distinguishable neurons in behaving mice is a technique with a rapidly growing appeal, particularly because it can be combined with gene targeting techniques. This methodology is deemed essential for achieving a flexible and versatile coupling of molecular-genetic manipulations with behavioral and system level analyses of the nervous system. One major obstacle in obtaining this technological integration is the relatively high weight and bulk size of the available implantable devices for ensemble recordings as compared to the size of the animal. This imposes considerable physical stress on the animals and may prevent them from performing complex behavioral tasks for more than a few minutes. We developed a novel micro-drive which allows independent day-to-day positioning of up to 6 tetrodes in the mouse brain, with an extremely reduced weight and size. The system is based on an “exoskeleton” as its structural element, and allows a completely rectilinear path of the electrodes inside the drive and into the brain. Tests showed that mice can tolerate the chronically implanted device very well up to 12 weeks after implantation, while exhibiting normal behavior. Cell yields and stability obtained with this drive in two different brain areas (the hippocampus and orbitofrontal cortex) were comparable to those of traditional recording systems, usually applied to rats. The device may greatly expand possibilities to combine gene targeting and ensemble recording techniques, in behaviorally varied as well as cognitively demanding settings.

© 2008 Elsevier B.V. All rights reserved.

### 1. Introduction

Over the last 15 years, gene targeting techniques have become a major tool for systems neuroscience, particularly in the study of behavior and physiology, and they usually rely on the mouse as the animal model of preference. Compared to other techniques for manipulating the molecular and neurochemical state of the brain, gene targeting has the potential to offer greater spatiotemporal specificity and uniformity in the spatial distribution of the genomic manipulation across the brain areas of interest (Chen and Tonegawa, 1997). Recent technological advances have increased the attractiveness of gene targeting methods, by restricting the manipulation to a targeted brain area (Tsien et al., 1996), or by temporally controlled, reversible induction, or knockout, of gene expression (Mansuy and Bujard, 2000; Nakashiba et al., 2008).

Neural ensemble recording – the simultaneous recording of the electrical activity of groups of neurons with single-unit isolation

– in behaving, freely moving animals, has been a key technique in the study of the neural basis of cognition and behavior. Neural ensemble data have informed our current concepts of some of the most important cognitive domains. A classic example is the spatial cognition and navigation system. Our knowledge of this system is largely based on data about spatial correlates of the firing activity of cell ensembles in the hippocampal system and related structures of rodents, most frequently rats, and their ensemble dynamics (for reviews, see, e.g. Leutgeb et al. (2005), McNaughton et al. (2006), O'Keefe and Burgess (2005), Bird and Burgess (2008)). The results obtained with these techniques have recently been at least partially confirmed by data collected in human patients (Ekstrom et al., 2003), and the application of ensemble electrophysiology in rats has been recently spreading to other cognitive domains and other parts of the brain.

So far, neural ensemble recording studies in mice have delivered some important successes (Nakazawa et al., 2002; McHugh et al., 1996, 2007; Kargo et al., 2007; Lin et al., 2006), often in combination with gene targeting (Nakazawa et al., 2004; McHugh et al., 1996), allowing to link genetically induced changes at the molecular level with their repercussion on activity at the neural

\* Corresponding author. Tel.: +31 20 5257618; fax: +31 20 5257709.  
E-mail address: [C.M.A.Pennartz@uva.nl](mailto:C.M.A.Pennartz@uva.nl) (C. Pennartz).

network level and behavior. For example, gene knockouts of NMDA subunits responsible for synaptic plasticity specific to different hippocampal subregions, have been seen to cause degradation of the spatial selectivity of hippocampal place cells (Nakazawa et al., 2002; McHugh et al., 1996, 2007). Yet, the technique has remained significantly limited in either its behavioral applications or cell yields as compared to equivalent studies in rats.

One major hurdle in obtaining reliable ensemble recordings, with a sizeable number of simultaneously monitored units, has been that even the lightest of the currently available recording devices (at least among those with more than 2 tetrodes) is still heavy and large relative to the tiny size of the mouse. Mouse recording devices in use today are usually scaled-down versions of instruments designed for the rat, an animal about 10 times the size of a mouse and proportionally stronger. With such devices, 1–6 independently movable electrodes can be typically implanted, yet they are relatively heavy, often exceeding 10% of the animal's body weight (e.g. 3.5 g for the device described by McHugh et al., 1996, or about 8 g for the device used by Yamamoto and Wilson, 2008). Even when the implanted mouse is not heavily impaired in its free movement through an environment, the weight of the electrode drive limits the range of feasible behavioral tasks to very basic ones, such as spatial exploration and foraging.

Moreover, the trade-off between weight and number of recording channels has hampered our ability to study juvenile or otherwise smaller mice (or other animals).

A more flexible and widespread applicability of ensemble recordings in mice requires designs that alleviate these problems. Here we present a novel micro-drive designed specifically for use in mice but also applicable in other small animals, and fulfilling the following requirements: (i) ultra-light weight (less than 2 g, or clearly less than 10% of a standard body weight of 30 g) and reduced size, so as to minimize additional, unnatural effort associated with head movement; (ii) compatibility with tetrodes, i.e., 4-way bundles of metal wire microelectrodes (McNaughton, 1983; O'Keefe and Recce, 1993), which can significantly improve recording yields (Wilson and McNaughton, 1993) and quality of signal discrimination (Gray et al., 1995; Harris et al., 2000); (iii) precise and independent day-to-day positioning of electrodes, without requiring forceful restraint of the animal during placement; (iv) compatibility with existing, commercially available electrophysiology data acquisition systems; (v) simple assembly procedures. In addition, (vi) the device must be re-usable multiple times.

Thus, we aimed at producing a micro-drive with a recording performance at least on par with the current state-of-the-art (McHugh et al., 1996; Nakazawa et al., 2002), but considerably lighter. Our device is essentially based on a lead screw-driven electrode positioning system (Ainsworth and O'Keefe, 1977), but introduces several innovations in design and materials. Most importantly, the layout of the electrode-supporting cannulae in the drive is linear and parallel, thus minimizing friction during electrode movement. Furthermore, we made use of a flexible printed circuit

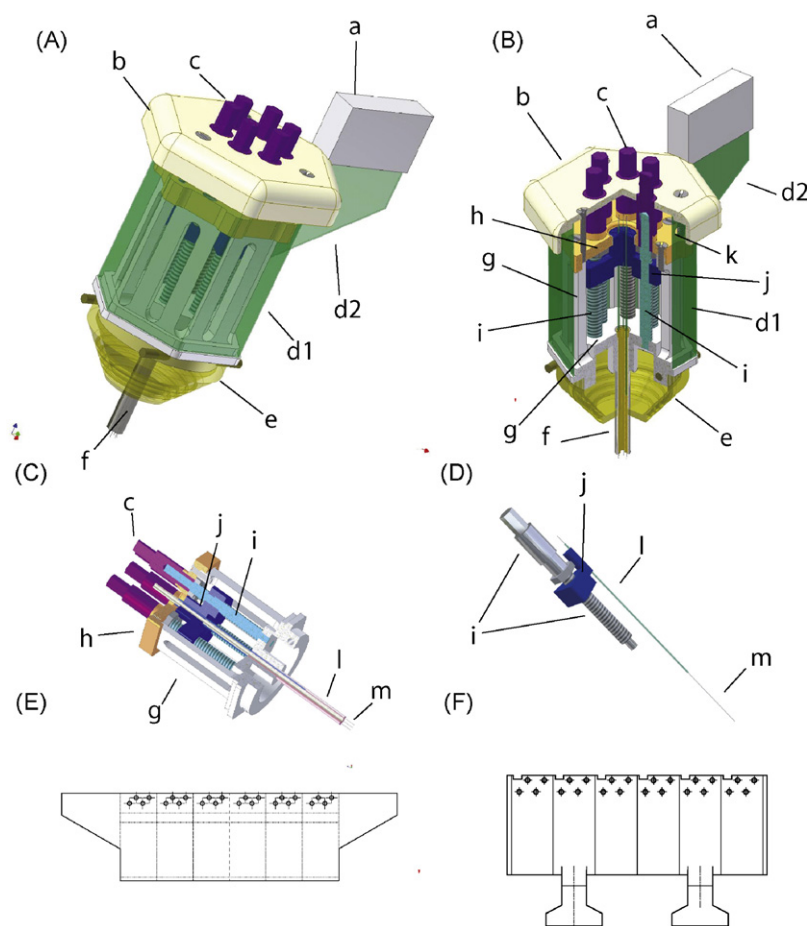


**Fig. 1.** Schematics of the micro-drive. (A) Outside view and (B) inside view and electrode holders, with tetrodes. (C) Inside view with the upper cap and the bottom shell removed. (D) Detail of the mechanism for tetrode depth adjustment including the screw piece, the electrode holder and the tetrode. (E) Scheme of the flexprint (unfolded) for the 4-tetrode configuration. (F) Scheme of the flexprint for the 6-tetrode configuration. List of symbols—*a*: Headstage connector. *b*: Upper cap. *c*: Screw heads. *d1*: Flexprint. *d2*: Flexprint flaps, connectors for headstage pre-amplifiers. *e*: Bottom shell. *f*: Guide cannula bundle. *g*: Drive body (width: 9 mm). *h*: Drive core. *i*: Screw parts (length = 13 mm). *j*: Electrode holder. *k*: Connection holes for individual tetrode wires. *l*: Silica capillary. *m*: Tetrode. Total height of the device (including cannula bundle: 23 mm). (For interpretation of the references to color in this figure legend, the reader is referred to the web version of the article.)

board folded around the micro-drive relaying all electrode signals to headstage and cables.

## 2. Materials and methods

### 2.1. Drive design

The drive design followed the tradition of multi-electrode, screw-controlled micro-drives for chronic implants (Nakazawa et al., 2004); however, the design introduced several new principles, aimed at reducing the weight and size as much possible, as well as at simplifying drive assembly and re-use.

The structural elements (Fig. 1) of the drive include an outer shell, resembling the Lantern placed on top of many classical church domes, and a core piece manufactured in PEEK (Eriks, Alkmaar, Netherlands), a plastic that was chosen for its superior mechanical characteristics including strength-to-weight ratio. The outer shell is composed of three pieces, first, a *body* (marked in Fig. 1 as *g*), in the form of a hexagonal prism, with an open top side and an aperture on the bottom side to house the cannula bundle (see below). Second, the shell contains an inverted cone-shaped, hollow *base* (*e*), that snaps on a lip on the bottom side of the body, with a central hole for the cannula bundle. Third, the shell includes an upper *cap* (*b*) screwed on the drive body. A *core* piece (*h*) is positioned within the shell and this holds the *screw pieces* in place; it is fastened from the top on the sides of the drive body with 6 micro-screws (Jevveka, Amsterdam, Netherlands).

The screw pieces (Fig. 1D) are the key mechanical parts of the drive: they are used to adjust the electrode depth below the cortical surface. Each screw (*i*) has a top part shaped with a square profile (*c*), and a threaded bottom part. It is attached to the core piece by means of a micro-nut placed underneath the core piece, so that it is free to turn. The bottom tip of the screw is anchored in the bottom part of the drive body, preventing the screw from moving, except for rotation around its axis. Screw pieces are turned manually by means of a turning tool fitting the square top of the screws. The electrode holder piece (*j* in Fig. 1), also manufactured in PEEK, has the profile of a triangular prism, such that 6 of these elements can be arranged in a hexagon shape, which fills the interior of the drive body (*g*). The holder (*j*) has a threaded hole through its vertical axis, hosting the screw piece. Its orientation is kept constant by one of its sides sliding along the inner surface of the drive body. Therefore, as the screw piece is turned, the electrode holder will move up and down. The tip of the electrode holder has a vertically oriented hole fitting a piece of polyimide-coated fused silica capillary tubing (*l*; Polymicro, Phoenix, Az; model TSP065125, 125  $\mu\text{m}$  outer diameter, 65  $\mu\text{m}$  inner diameter), containing the tetrode. A bundle of six 30-ga hypodermic cannulae in a hexagonal shape traverses the drive body and base (*e*). As an individual electrode holder moves up and down, each of the 6 capillary-tetrode combinations slides inside one of the cannulae. The tetrodes exit the drive from the bottom tip of the cannulae, which, after surgical implant, touch the subject's brain (diameter of the bundle at the tip: 1.2 mm). This mechanism is considerably simplified and has a reduced number of parts with respect to the existing designs. For example, previous designs needed a second tubing attached to the electrode holder to prevent the capillary and tetrode from buckling (Gothard et al., 1996; Lansink et al., 2007). Because in the new design the path of the silica capillary is completely rectilinear, and friction is minimal, the need for this auxiliary tubing is obviated. Moreover, the drive body itself keeps the electrode holder in the proper horizontal bearing, effectively replacing the second supporting rod that was required in the progenitor drive designed for rats (Gothard et al., 1996; Lansink et al., 2007). The current drive mechanism allows each tetrode about 5 mm of useful travel range, covering the entire dorsoventral extent of a typical mouse brain. An extension of the

travel range, in order to reach deep brain structures in larger animals, is possible by increasing the drive height. Each 360° turn of the screw lowers the tetrode by 250  $\mu\text{m}$ .

At the topside of the electrode holder, the tetrodes exit the capillary. At this end, they are split in the four constituent wires for electrical connections. Connections are accomplished through a custom-designed flexible printed circuit board (*flexprint*; *d1*–*2* in Fig. 1). Flexprints are folded in a hexagonal shape (*d1*), and they wrap around the drive body. Connection receptacles (*k*) for the tetrode wires are located at the upper lip of the flexprint, which protrudes above the drive core. We realized two versions of the flexprint: the first (Fig. 1E) connects to one 16-channel headstage pre-amplifier HS-16 (Neuralynx, Bozeman, MT) and can accommodate 4 tetrodes. The second one (Fig. 1F) connects to 2 HS-16 amplifiers and can accommodate 6 tetrodes. The headstage pre-amplifiers are connected to the flexprint via micro-connectors (Omnetics Connectors Corporation, Minneapolis, MN; custom ordered: NPD-18-FF-GS, Nano Dual Row Male, 18 contacts, marked with *a* in Fig. 1). The headstage connectors are mounted on flaps of the flexprint (*d2*) protruding from the lateral side of the drive. The upper cap (*b*) is screwed on the drive core with micro-screws (same type as above) and holds the flexprint in place. The flexprint is lightly glued to the drive shell at the bottom with cyanoacrylate.

The total weight of the drive (excluding headstages but including flexprint) was 1.8 g. Fig. 2 shows the ready-to-implant drive connected to headstages in the 6-tetrode and 4-tetrode configuration.

### 2.2. Drive assembly procedure

Tetrodes are prepared according to the procedure described by Gray et al. (1995). Briefly, four threads of polyimide-insulated, 13  $\mu\text{m}$  diameter nichrome wire (Kanthal, PalmCoast, FL) are twisted together and the insulation is melted by heating until the bundle is stably fused together. At one end, the wires are left unbundled so that they can diverge to their electrical contacts.

The cannula bundle making up the bottom end of the drive is realized by six 10 mm pieces of 30-ga hypodermic tubing, held together at the base by a stainless steel ring (3 mm long, 1.2 mm diameter). A shorted piece of cannula is placed at the center of the bundle as a spacer.

Six pieces of silica capillary, 14–16 mm in length, are inserted in each of the holes in the electrode holders (*j* in Fig. 1) and glued to them with cyanoacrylate gel. The electrode holders are then inserted over the screws so that they form a hexagon, with the capillaries laying in parallel at the center of the hexagon. The cannula bundle is inserted through the shell base and next into the body of the shell; the shell base is then snapped on the drive body, so that the outer ring of the bundle protrudes downwards from the bottom

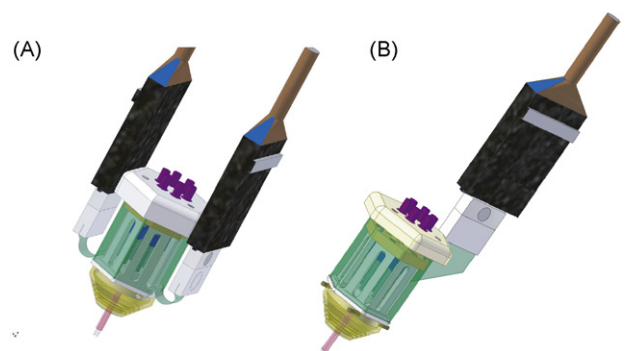


**Fig. 2.** The micro-drive connected with the headstages. (A) The 6-tetrode configuration. (B) The 4-tetrode configuration. (For interpretation of the references to color in this figure legend, the reader is referred to the web version of the article.)

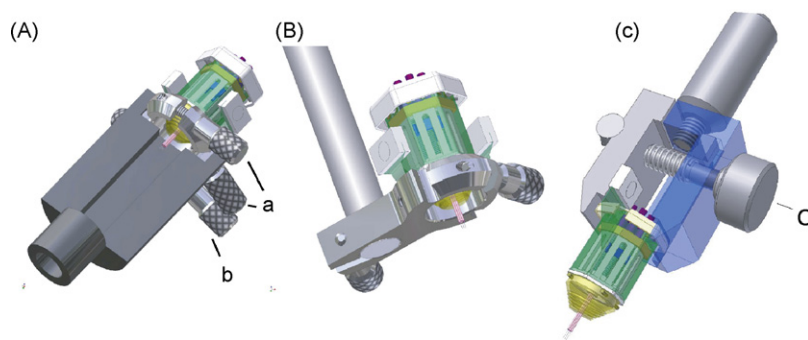


**Fig. 3.** The micro-drive holders. (A) The loading holder in its full configuration. The holder includes a base piece, intended to protect the electrode wires during drive assembly. *a*: Set screws securing the micro-drive to the holder. *b*: Screws attaching the base piece to the holder. (B) The same holder with the base detached, in the configuration for gold plating of electrode tips. (C) The surgical holder. (The blue translucent surfaces denote parts of the holder and micro-drive that would normally be invisible from this angle of view.) (For interpretation of the references to color in this figure legend, the reader is referred to the web version of the article.)

of the shell base and the top ends of the cannulae are exposed inside the drive body. Next, the silica capillaries are carefully inserted each one in a cannula and the core piece is gently inserted from the top end into the drive body, and secured with 6 micro-screws. The flexprint is then wrapped around the outer surface of the drive.

At this stage, the top ends of the capillaries are accessible through the central aperture in the drive core. The insulating layer is removed from the top, unbundled end of the tetrode wire by brief exposure to a flame. Tetrodes can now be threaded through the capillary, and the exposed portion of the wire is inserted in the appropriate connection hole in the flexprint. Connections are established by micro-soldering and covered with conformal coating or nail polish for protection. As a last step, the tetrodes are glued to the bottom end of the silica capillaries with cyanoacrylate, and cut to the desired length. The tetrode tips are electrolytically gold-plated in a gold cyanide solution (Select Plating, Meppel, the Netherlands) to an impedance of 0.5–1.0 M $\Omega$  and next the tetrodes are retracted so that the tip is flush with the bottom end of the guide cannulae.

### 2.3. Drive accessories

Given the small size of the drive, custom-made tools are necessary for its assembly and surgical implantation. We realized two holders for the drive, one for use during the assembly procedure, the other for stereotaxic surgery. The assembly holder (Fig. 3A) is made from Polyacetate (Eriks, Alkmaar, Netherlands) and contains a metal ring that can be fastened onto the drive base by means of 2 set screws (*a*). The holder allows easy access to the drive top (from where the tetrodes are loaded) and to the bottom part of the drive with the protruding tetrodes. Moreover, the metal ring can be released from the rest of the holder by unscrewing the set screws (*b*) and connected, e.g. to a stereotaxic adapter, to allow dipping of the tetrodes in the gold-plating solution (Fig. 3B).

The surgical holder (Fig. 3C) can be fit on a standard stereotaxic manipulator. It consists of a clamp, operated by a spring-loaded thumb screw (*c*). After implantation on the animal's head, the holder can be released without applying force on the head.

### 2.4. Interfacing with the data acquisition system

The present version of the drive was fitted with connectors to interface with a Cheetah recording system (Neuralynx). In the four-tetrode configuration, the headstage cable (2 m in length) connects directly to the EEG reference/patch panel of the Neuralynx system. In the six-tetrode configuration, the two headstage cables connect to the patch panel through a modified Neuralynx slip-ring commutator. The two HS-16 headstages were chosen because they represented the lowest weight, Cheetah-compatible solution with a sufficient number of channels.

### 2.5. Surgery and tetrode positioning

In the first set of experiments, surgical levels of anesthesia were reached with a combination of ketamine (100 mg/kg body weight; *Nimatek*, Eurovet, Bladel, Netherlands) and Medetomidine (1 mg/kg body weight; *Domitor*, New York, NY) administered intraperitoneally as a bolus of 0.1 ml (diluted in saline) for a typical (30 g) mouse. If needed, anesthesia level was maintained during the surgery with booster injections of ketamine (50 mg/kg each time). In later experiments, animals were first sedated with subcutaneous Buprenorphine (3 mg/kg; *Temgesic*, Schering-Plough, Kenilworth, NJ), and 30 min later brought and kept at surgical levels of anesthesia with 1–3% isoflurane gas anesthesia. Anesthesia levels were controlled and adjusted by monitoring heart beat and respiration rate. Body temperature was controlled throughout anesthesia with a rectal probe and maintained at 36.5–37 °C with a closed-circuit thermal pad. Mice were attached to a stereotaxic apparatus (David Kopf Instruments, Tujunga, CA) through jaw bars and a mouth-piece. The skin and peri-osteal membrane were retracted, 5–6 bone screws (one used as ground) were implanted, and a craniotomy (about 2–2.5 mm diameter) was drilled at the appropriate stereotaxic coordinates (for the hippocampus: AP –2.0 mm, ML 1.0 mm from bregma, for the orbitofrontal cortex: AP 2.5 mm, ML 0.3 mm). The dura mater was dissected and the drive lowered until the bottom end of the cannula bundle made contact with the brain surface to ensure tetrode penetration in the brain, especially in the frontal lobe, where the dura is thicker. The craniotomy was sealed with a biocompatible Silastic elastomer (Kwik-Sil, World Precision Instruments, Berlin Germany) and the position of the drive was fixed with dental cement.

After surgery mice were administered 0.5 ml saline s.c. for rehydration, and 2 mg/kg Flunixin s.c. for analgesia. The effect of medetomidine, when applicable, was reverted by 1 mg/kg intraperitoneal atipamezole (*Antisedan*, Pfizer, New York, NY). Implanted mice were housed solitarily in special cages with an elevated ceiling.

In the week after the surgery, tetrodes were gradually lowered to the desired anatomical location, before recordings began. Depth was evaluated by keeping track of the number of screw turns operated, and when available, by signs in local field potentials (LFPs) and unit signals distinctive of certain brain areas (e.g. theta rhythm and sharp waves-ripples for hippocampal area CA1).

### 2.6. Data acquisition

Tetrode signals were unit-gain amplified by the headstage pre-amplifiers and relayed to amplifiers for single-unit and LFP recordings. For single-unit recording the signal was amplified 2000 times and band-pass filtered (0.6–6.0 kHz); waveforms from all four

channels of one tetrode were acquired (32 kHz sampling rate) and time-stamped each time the signal exceeded a manually selected threshold on one of the channels. LFP signals were amplified 2000 times, filtered between 1 and 475 Hz and continuously acquired at 2 kHz sampling rate. Normally, a skull screw on the side contralateral to the implant was used as a reference for LFPs, and one tetrode (targeted to a location devoid of units and near the area of interest) was used as reference for single-unit signals, leaving 3 or 5 tetrodes available for single-unit recordings for, respectively, the 4-tetrode and the 6-tetrode version of the drive. Alternatively, a separate, non-movable reference electrode wire may be implanted and used as reference. Single-unit data were pre-processed with either BBClust (P. Lipa, University of Arizona, Tucson, AZ) or KlustaKwik (K. Harris, Rutgers University, Newark, NJ) for automated spike clustering. Spike sorting results were manually refined using MClust (A.D Redish, University of Minnesota, Minneapolis, MN) or Klusters (Hazan et al., 2006). Clusters with less than 0.2% inter-spike intervals inferior to 2 ms were used for the analyses.

For Experiment 1, the position of the mouse in its environment was tracked by two different methods: the position of an LED on the headstage pre-amplifier was tracked by a CCD camera placed above the arena, and registered by the Cheetah recording system. This system had the disadvantage of making large parallax errors, because of the elevated position of the LED on top of the headstage (about 4 cm from the mouse's head). A more precise determination of the mouse position was obtained with Ethovision XT image analysis software (Noldus, Wageningen, The Netherlands), which was able to extract position and orientation of the mouse body from video images, both offline and in real time.

From the identified cells that yielded at least 50 spikes during a recording session, firing patterns were processed to produce perievent time histograms (PETHs) and firing rate maps. Firing rate maps represent a cell's local firing rate as a function of the animal's spatial position in an environment. Only spikes emitted while the animal was running at least 4 cm/s were included in the analysis.

### 2.7. Subjects and behavioral procedures

All experiments were conducted according to local and national regulations, and with permission from the Institution's Animal Wel-

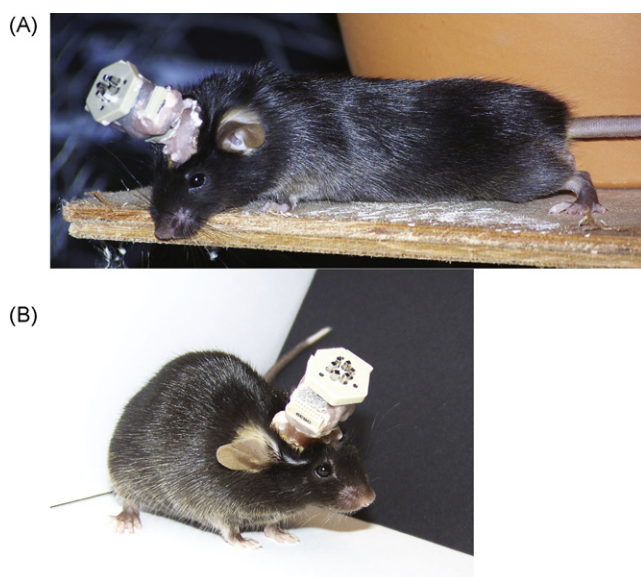


**Fig. 4.** Freely behaving implanted mice. (A and B) Photographs of mice implanted with the Lantern drive, which does not significantly affect their normal posture or movement. (For interpretation of the references to color in this figure legend, the reader is referred to the web version of the article.)

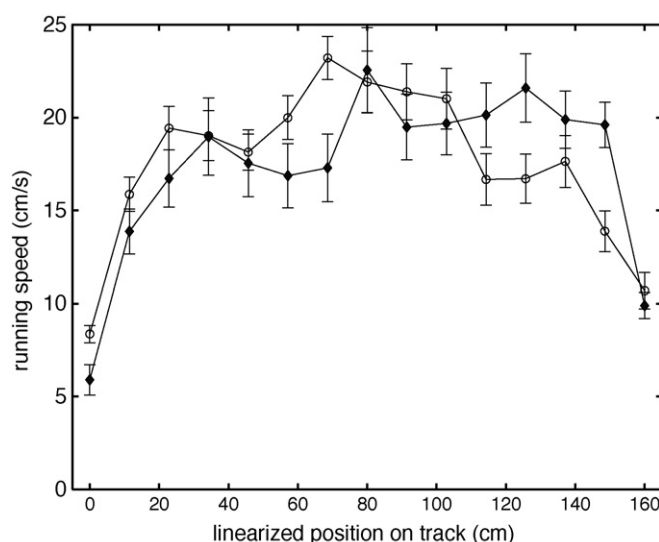


**Fig. 5.** Running speed profile for implanted and non-implanted mice. Average running speed as a function of position on the track for implanted and tethered mice (filled diamonds) and non-implanted mice (open circles) shuttling back and forth on a circular track for food reward. The animals were juveniles with a weight of 22–24 g. The analyzed sessions started with the second overall exposure of the animals to the maze. Data from 1 implanted mouse (four sessions) and 2 non-implanted mice (4 sessions). Error bars represent S.E.M.

fare Committee. The function and versatility of the drive were tested in two experiments, on a total of 8 mice of different strains (C57Bl6, 129/Sv) and age (3 weeks–4 months at surgery, 17–35 g weight; 7 of these mice were below 22 g and 21–28 days old and thus considered juvenile). The subjects were allowed to acclimatize to the colony rooms for at least 2 weeks before the beginning of experimental procedures, and were housed on a reversed 12 h/12 h light cycle (lights on at 8:00 p.m.). Before implantation, mice were housed in groups, and given ad lib food and water except for the situations specified below. Here we report two experiments targeting different brain areas and using different behavioral tasks.

### 2.8. Experiment 1—spatial navigation in circular track

Upon mild food restriction (access to food was not allowed for 5 h prior to each training or recording session), 6 C57Bl6 mice were

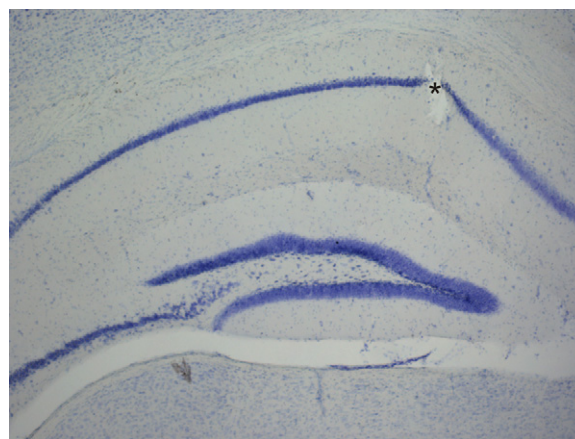


**Fig. 6.** Histological verification of tetrode placement. Microphotographs of Nissl stained hippocampal sections, showing a tetrode track (indicated by asterisk) terminating in, or slightly ventral to, the CA1 pyramidal layer. (For interpretation of the references to color in this figure legend, the reader is referred to the web version of the article.)

left resting in their home cage, positioned at the center of the experimental arena, for 15–20 min were placed on a circular track (60 cm diameter, 8 cm width), where they alternated between clockwise and counter-clockwise laps between two contiguous locations separated by a barrier and baited with sucrose pellets. The task session lasted for 20–40 min, or until the animal stopped running consistently. After each session, mice rested for another 15–20 min in their home cage. After surgical implantation and recovery, the same procedure was followed, and recordings were performed during the full task and rest periods, with the data from the rest intervals used for calibration and validation of the spike discrimination procedure.

### 2.9. Experiment 2—learning the motivational significance of reward-predicting stimuli

One 129/Sv mouse was water restricted during its inactive period, and trained in a reward-devaluation task. The training took place in a Skinner box equipped with a sound generator and a fluid well for application of reinforcing sucrose solution. A training session consisted of 25 trials. Each trial began with an inter-trial interval (ITI) of variable length (37.5–39.5 s), followed by a sound cue of 500 ms duration. Then, after a delay of 2 s, a reward of 10  $\mu$ l of 10% diluted sweetened condensed milk was delivered in the fluid well. The availability of reward was indicated by a small cue light

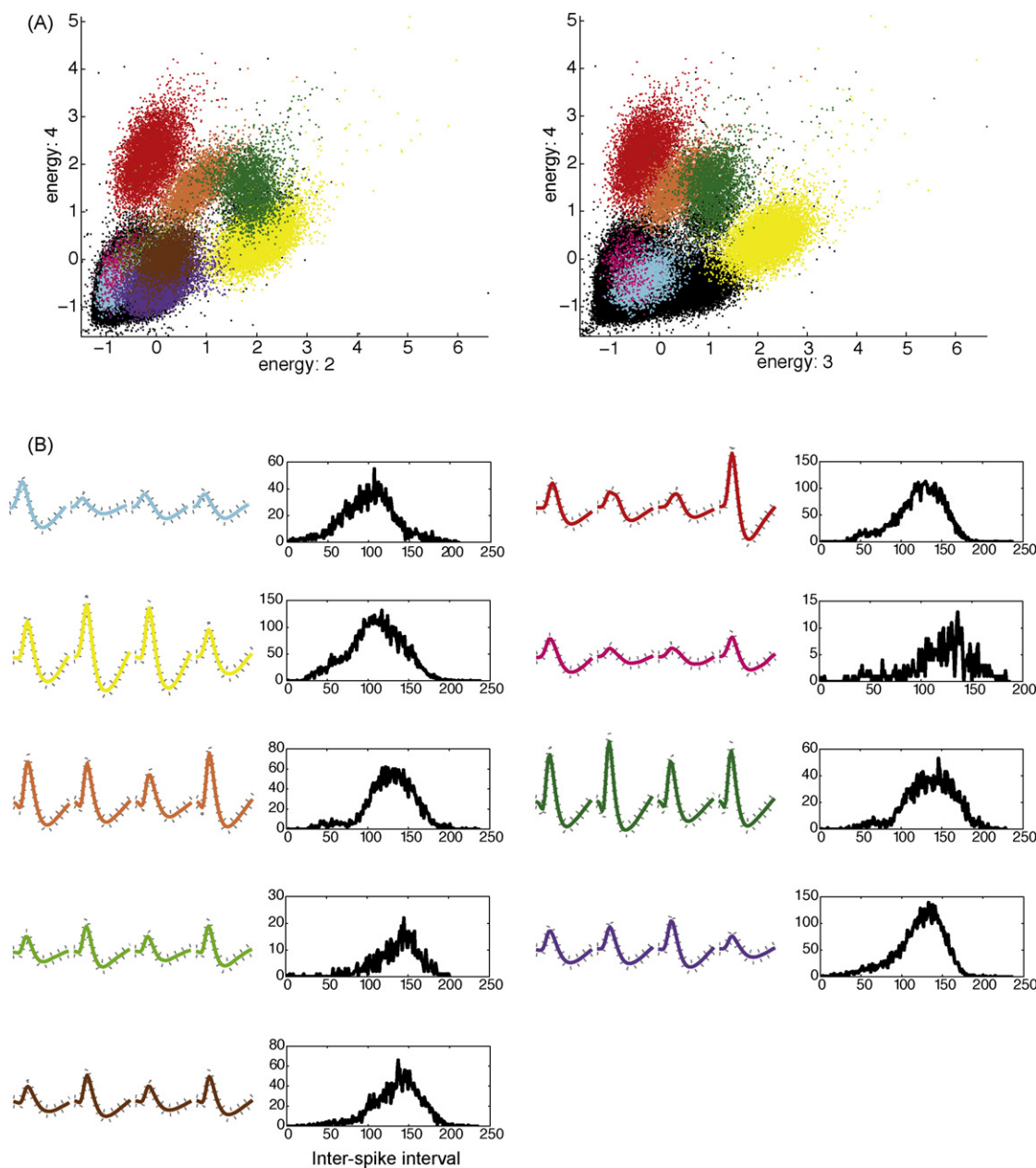


**Fig. 7.** Examples of discriminated spike waveforms from the orbitofrontal cortex. (A) Two example scatterplots of the amplitudes of all simultaneously recorded events from one tetrode placed in the orbitofrontal cortex. “Energies” on channels 2 and 4 (left) and 3 and 4 (right) of the tetrode are displayed. Nine single units were discriminated on this tetrode. (B) The average waveforms (with S.E.M.) on the 4 channels for all 9 discriminated cells, and the inter-spike interval histograms; colors correspond to the spike cluster in (A). To the right of each set of four waveforms, inter-spike interval histograms for each of the discriminated units are plotted. Plots were created with the MClust program by A.D. Redish. (For interpretation of the references to color in this figure legend, the reader is referred to the web version of the article.)

positioned above the well. The reward was available in the well for 8 s, if it was not consumed after that time, it was flushed away.

### 2.10. Histology and drive recycling

After recordings, electrolytic lesions were procured at the recording sites by passing 5  $\mu$ A of current for 5 s through one lead of each tetrode. Twenty-four hours later, the mouse was intracardially perfused with saline, followed by 4% paraformaldehyde saline. The brain was extracted from the skull and 40  $\mu$ m sections were cut and Nissl-stained. The drive was disassembled and residues of dental cement and cyanoacrylate were removed with acetone. If needed, debris on the disassembled drive was removed in an ultrasound cleaner. We have re-used the same drive at least 5 times with no discernible sign of tear (except small dents in the outer part of the drive), and we anticipate that each drive may be used at least 10–20 times.

## 3. Results

### 3.1. Behavior and biocompatibility of the drive implant

Mice recovered from surgery in 2–3 days maximum. The drive weight and torque were very well tolerated, and mice exhibited a range of normal behaviors including running, eating, drinking, grooming and rearing (Fig. 4). After surgery, mice stabilized their body weight in a few days. Already two days after surgery, even juvenile mice ( $N=7$ ; weight of 17–22 g, age of 21–28 days postnatally at surgery) could move quite naturally, including running on a circular track (Supplementary movie 1) and climbing over obstacles (Supplementary movie 2), while connected to the headstage pre-amplifiers and tether cables. Mice gained weight steadily, compatible with normal development. On a circular track, implanted and tethered mice could run with a speed that closely matched that of un-implanted mice of similar age, weight and training stage

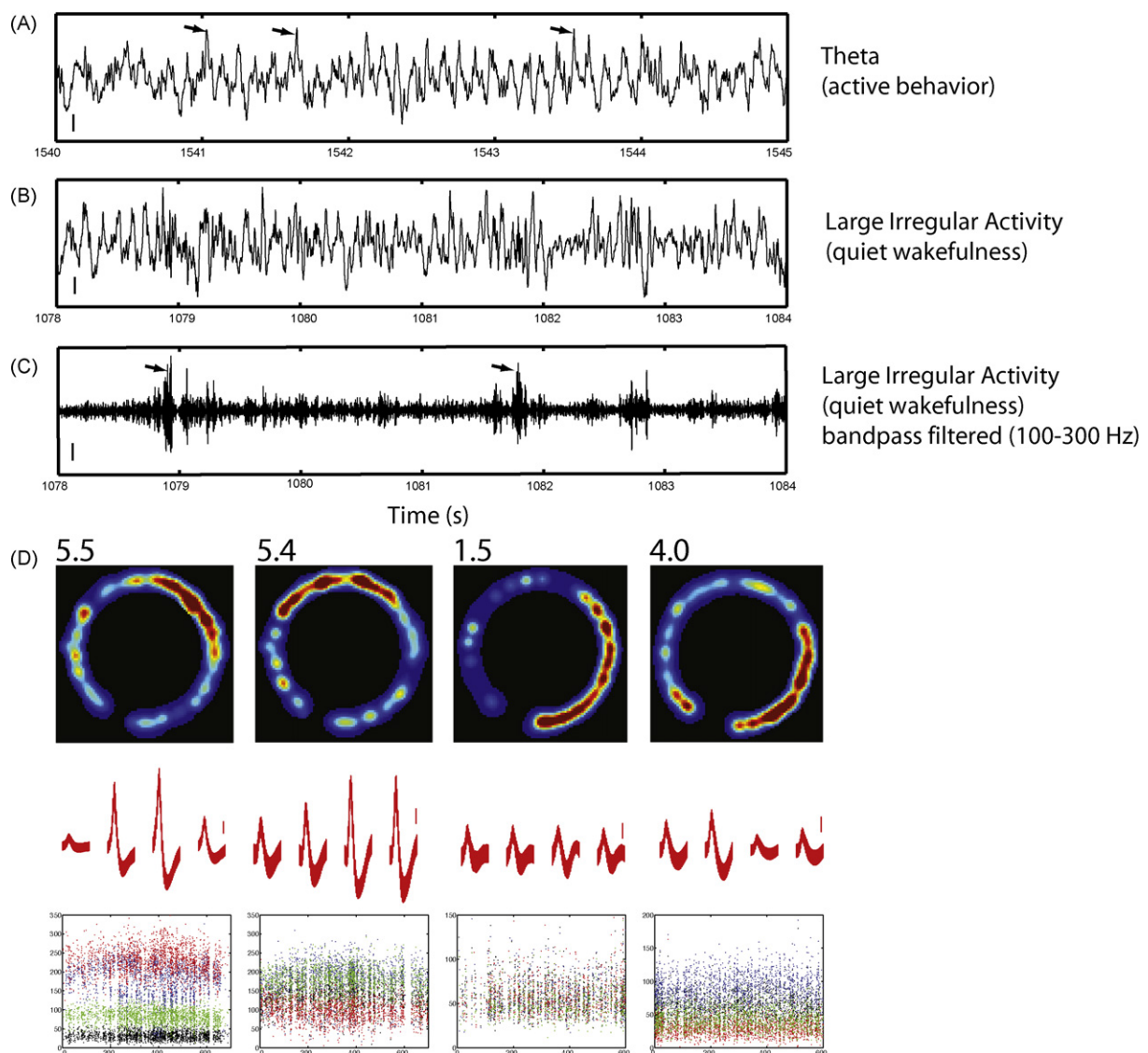


**Fig. 8.** Hippocampal recordings and spatial correlates of CA1 cell firing patterns on the circular track. (A) Five-second excerpt of hippocampal local field potential recorded while the rat was running, showing theta ( $\sim 8$  Hz) oscillations and gamma spikes (arrows). (B and C) Excerpts of hippocampal local field potential recorded during large irregular activity, shown as wide-band (B) and bandpass (100–300 Hz) filtered signals (C). Sharp-wave ripple complexes (arrows) are visible. Both ripples and large irregular activity are hallmarks of quiet wakefulness and slow-wave sleep. Calibration bars: 0.1 mV in A and B, 0.04 mV in C. (D) Top row: Firing rate maps on the circular track for 4 cells recorded simultaneously showing the relative firing rate as a function of the mouse's spatial position on the track. Middle row: The average waveforms for the four tetrode channels (error bars: standard deviation; calibration bar: 40  $\mu$ V). The numbers on top of each graph indicate the peak firing rate for each cell (in Hz). Bottom row: Scatter plot of the peak amplitude in microvolts of the waveform of each on the four channels (depicted, respectively, as black, blue, red, green dots; y axis) vs. the time of emission during the recording session (x axis, in seconds). (For interpretation of the references to color in this figure legend, the reader is referred to the web version of the article.)

(Fig. 5). Most mice wore the implant for at least one month and with a maximum of 12 weeks, and experiments were terminated only as the tetrodes reached the ventral border of the brain structure of interest. No implants were prematurely terminated because of a loss of drive adhesion to the skull of the mouse.

### 3.2. Histology

Nissl stains revealed tetrode tracks and end locations in each of the targeted areas. We verified that our estimates of electrode depth based on tracking screw turns were accurate within 200–300  $\mu\text{m}$ , a level of precision that is comparable with that obtained in rats with the traditional systems (Fig. 6).

### 3.3. Electrophysiological signals—single-unit signals

Recordings yielded a maximum of 12 discriminated units simultaneously recorded from hippocampal area CA1 per tetrode, and of 11 cells from the orbitofrontal cortex, with typical yields of 4–8 cells per tetrode in both areas (Fig. 7).

### 3.4. Electrophysiological signals—local field potentials

Signals from the CA1 subfield clearly showed the main features of the hippocampal EEG, including sharp waves/ripple complexes during immobile wakefulness, theta rhythm during locomotion and “gamma spikes” during active behavior that are characteristic of the mouse hippocampal LFP (Buzsáki et al., 2003) Fig. 8A shows a 5 s excerpt recorded while the animal was active. The characteristic theta rhythm (8 Hz) is clearly visible. Moreover, the “gamma spikes” typical of mouse hippocampus are present (indicated by arrows). The traces in Fig. 8B and C show a 5 s excerpt recorded during period of quiet wakefulness. Hippocampal ripple oscillations are visible, and can be better appreciated in the 100–300 Hz band-pass filtered signal (arrows in Fig. 8C).

### 3.5. Behavioral correlates of hippocampal ensembles

We recorded and analyzed a total of 91 single units from hippocampus in 6 sessions on the circular track.

On the circular track, several CA1 cells showed spatial selectivity, with place fields covering 30–50% of the track, compatibly with what has been previously demonstrated for mouse hippocampal place cells (Fig. 8D). Spike waveforms for these cells reached in some cases 250–300  $\mu\text{V}$  amplitude (peak-to-valley), which remained stable during the recording session in the maze (Fig. 8D).

### 3.6. Behavioral correlates of orbitofrontal neurons

We recorded a total of 261 single orbitofrontal neurons in 15 sessions. The combined activity of these cells correlated with nearly every element of the task: sound cue, reward consumption, both sound cue and reward consumption, delay period, both cue and delay period, jaw movement, and general movement. A typical neuron showing enhanced activity to the conditioned sound cue is displayed in Fig. 9A and B. This neuron had increased cue-related activity only in trials in which the reward was consumed, but the neuron was less responsive to the cue in trials without reward consumption. It is possible that the loss of cue responses during the omission trials is due to an increased satiation and concomitant loss of motivation, but this interpretation should be investigated further.

These data validate the performance of the drive in recordings in deep cortical structures, and in behavioral situations requiring mice to interact with automated feeders and other mechanical parts.

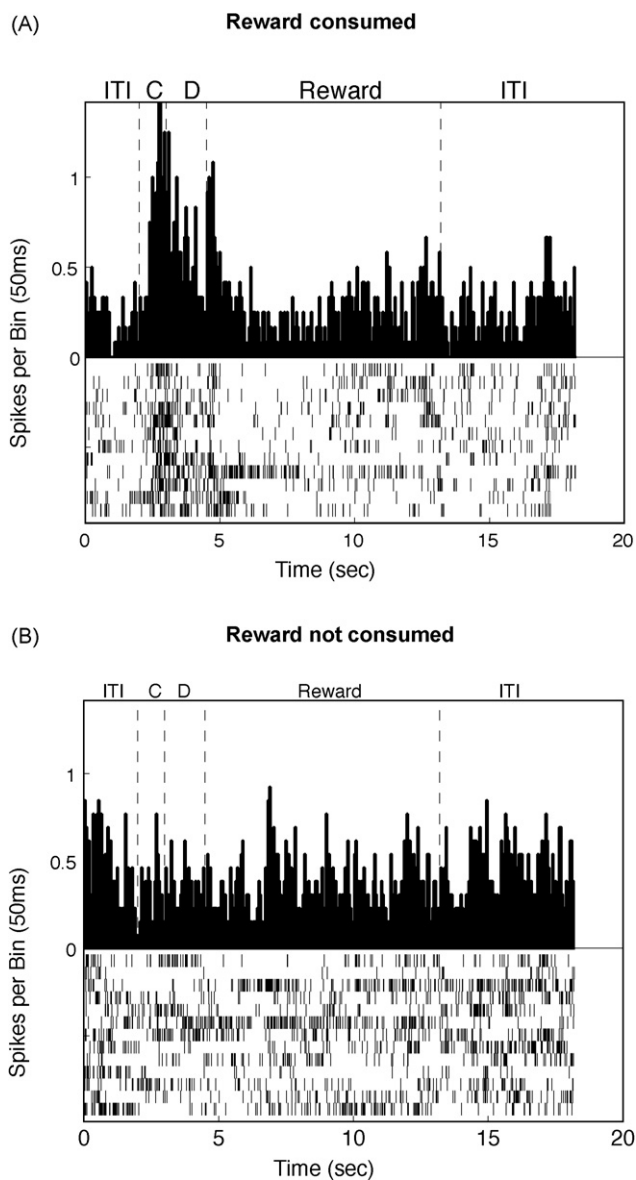


**Fig. 9.** Behavioral correlates of single-unit firing pattern recorded from the orbitofrontal cortex. (A) and (B) Peri-Event Time Histogram and spike rasters for individual trials for the activity of one example neuron, which responded with elevated firing rate to the auditory cue for trials in which the reward was consumed (A), but not for those in which the reward was not consumed (B). C: Cue period. D: Delay period.

## 4. Discussion

Several devices have been developed to enable single-units neural recordings, in small animals such as mice and song birds. The early technology for ensemble recordings in mice (McHugh et al., 1996) made use of adaptations of technologies intended for rats and other larger animals. More recent attempts brought, on the one hand, some original designs mainly aiming for a weight and size reduction (Jeantet and Cho, 2003) whereas, on the other hand, designs were introduced that privileged a larger number of channels, with a heavier and bulkier result, and without independently movable electrodes (Lin et al., 2006).

With respect to the former type of drive, which housed 1 or 2 tetrodes (Jeantet and Cho, 2003), our design provides a much larger number of recording channels, up to 24, grouped in 6 tetrodes. With respect to the latter type, the current design provides indepen-

dently movable tetrodes, and apparently a less bulky format (cf. Lin et al., 2006, their Fig. 2).

The strong points of the device presented here are its ultra-low weight and size, the large number of channels (24, in 6 tetrodes), the possibility for independent adjustment of the electrodes, the simple assembly procedure, and the linear path of the tetrode/guide capillary complex, while attaining roughly the same recording performance as the heavier 6-tetrode drives previously described in the literature (e.g. McHugh et al., 1996, 2007; Lin et al., 2006).

A weight of 1.8 g is comparable with those systems employing a much smaller number of channels (Jeantet and Cho, 2003), and much lighter than other devices comparable in terms of recording channels (McHugh et al., 1996). A low weight proves to be crucial for mice being able to tolerate the drive with relative ease, and to perform behavioral tasks without excessive physical effort and stress. Certainly, the weight of the pre-amplifier set and tethers is also important in determining the mouse's freedom of movement, but the gravitational force of these parts is relieved by a cable suspension system, and apparently the mouse was well capable of movement despite the remaining momentum (Fig. 5 and supplementary movies). Although the mice that were chronically recorded with the Lantern were able to perform several effortful tasks with relative ease (Fig. 9, and supplementary movie 2, we do note that comparative studies using different types of recording devices in mice performing the same set of tasks would be needed to draw strong conclusions about the effect of each drive on naturalistic behaviors.

Moreover, the device proved suitable for ensemble recording on juvenile mice of about 3 weeks of age and a body weight down to 17 g. To our knowledge, these are the lightest freely moving animals from which a sizable cell ensemble (15–20 units) has been simultaneously recorded. This may open up the possibility of performing ensemble recording very early in development in rats as well as mice.

A considerable rethinking of previous models of multi-tetrode drives made it feasible to reduce drive dimensions relative to the traditional prototype for rats and eliminate some guide cannulae and supporting rods by making use of the wall of the drive body as a support for the tetrode-manipulating mechanism. Furthermore, by reducing friction due to the linear electrode path the drive overcame the need for a drive core of solid plastic, which has now been replaced by a light-weight, 3-component “exoskeleton” (i.e., a shell composed of the drive body, core piece and base). The use of PEEK as the material for all structural parts of the drive further allowed us to decrease the weight. Other gains in weight and size come from the use of flexprints, which are thinner and lighter than regular printed circuit boards, and allowing users to exploit the space to the sides of the drive for making electrical connections.

Despite the miniaturized dimensions of the device, the assembly procedure is at least as fast as for a traditional rat micro-drive (Gothard et al., 1996; Lansink et al., 2007). This is due to the reduced number of components and the omission of a time-consuming procedure for bending and routing of curvilinear elements (guide cannulae, etc.). After some practice, an operator can easily carry out the assembly of a micro-drive in a working day. Drive recycling is also rapid, thanks to the fact that most of the dental cement used for surgical implant is attached to the shell base, so that the other parts do not need any deep cleaning.

The linear electrode path, and the consequent reduction of friction, are also a factor increasing the reliability and durability of the implanted drive, preventing cracks in or breakage of the assembly of holder, guide tube and tetrode, which may be a cause of loss of functioning electrodes after implant. The positioning system allows for about 5 mm of useful travel, adequate for reaching virtually all parts of the mouse brain. The low weight and height (and therefore mechanical torque on the skull) also improve the durability of the

drive attachment to the skull, which is so thin in the mouse that it becomes a critical factor for chronic recordings.

Signal quality and stability proved as good with this system as with more conventional rat drives, although admittedly we did not compare rat and mouse recordings systematically. Cells could be discriminated and recorded for a full recording session lasting 1–2 h, both in orbitofrontal cortex and hippocampus, and once in place, the electrodes stayed in a cell-rich location such as the pyramidal cell layer of hippocampal area CA1 for several days, without a need for further positioning.

Mouse CA1 cells have spatial correlates similar to those described in rats, however, as has been previously described (McHugh et al., 1996; Nakashiba et al., 2008), they tend to exhibit broader place field and lower spatial selectivity. Our circular maze results are compatible with this picture, proving that our recording device can successfully capture behavioral correlates of neural activity in the mouse hippocampus.

The current design also lends itself to several extensions and modifications, such as wireless transmission components. Micromotors may be utilized to position the electrodes in a computer-controlled manner, so that manual intervention on the animal is no longer needed to optimize electrode depth. These and other possibilities are currently under study in our lab and elsewhere (Cham et al., 2005; Yamamoto and Wilson, 2008). However, the focus of the device presented here and of its future evolutions rests on the reduced weight and size.

In conclusion, the Lantern has the potential of significantly enhancing the feasibility and yield of ensemble recordings in freely moving mice, bringing these much closer to what possible in the rat, the current species of choice for multi-neuron recordings. The benefits may extend to the investigation of juvenile rats and mice and other small animal species, like birds, or small mammals other than mice (e.g. bats—Ulanovsky and Moss, 2007) which may significantly modify our knowledge of a diversity of brain systems and cognitive functions, mostly based on only a few model species.

## Appendix A. Supplementary data

Supplementary data associated with this article can be found, in the online version, at doi:10.1016/j.jneumeth.2008.12.024.

## References

- Ainsworth A, O'Keefe J. A lightweight microdrive for the simultaneous recording of several units in the awake, freely moving rat. *J Physiol* 1977;269:8P–10P.
- Bird CM, Burgess N. The hippocampus and memory: insights from spatial processing. *Nat Rev Neurosci* 2008;9:182–94.
- Buzsáki G, Buhl DL, Harris KD, Csicsvari J, Czéh B, Morozov A. Hippocampal network patterns of activity in the mouse. *Neuroscience* 2003;116:201–11.
- Cham JG, Branchaud EA, Nenadic Z, Greger B, Andersen RA, Burdick JW. Semi-chronic motorized microdrive and control algorithm for autonomously isolating and maintaining optimal extracellular action potentials. *J Neurophysiol* 2005;93:570–9.
- Chen C, Tonegawa S. Molecular genetic analysis of synaptic plasticity, activity-dependent neural development, learning, and memory in the mammalian brain. *Annu Rev Neurosci* 1997;20:157–84.
- Ekstrom AD, Kahana MJ, Caplan JB, Fields TA, Isham EA, Newman EL, Fried I. Cellular networks underlying human spatial navigation. *Nature* 2003;425:184–8.
- Gothard KM, Skaggs WE, Moore KM, McNaughton BL. Binding of hippocampal CA1 neural activity to multiple reference frames in a landmark-based navigation task. *Journal of Neuroscience* 1996;16:823–35.
- Gray CM, Maldonado PE, Wilson M, McNaughton B. Tetrodes markedly improve the reliability and yield of multiple single-unit isolation from multi-unit recordings in cat striate cortex. *J Neurosci Methods* 1995;63:43–54.
- Harris KD, Henze DA, Csicsvari J, Hirase H, Buzsáki G. Accuracy of tetrode spike separation as determined by simultaneous intracellular and extracellular measurements. *J Neurophysiol* 2000;84:401–14.
- Hazan L, Zugaro M, Klusters Buzsáki G. NeuroScope: a free software suite for neurophysiological data processing and visualization. *J Neurosci Methods* 2006;155:207–16.
- Jeantet Y, Cho YH. Design of a twin tetrode microdrive and headstage for hippocampal single unit recordings in behaving mice. *J Neurosci Methods* 2003;129:129–34.

- Kargo WJ, Szatmary B, Nitz DA. Adaptation of prefrontal cortical firing patterns and their fidelity to changes in action-reward contingencies. *J Neurosci* 2007;27:3548–59.
- Lansink CS, Bakker M, Buster W, Lankelma J, van der Blom R, Westdorp R, et al. A split microdrive for simultaneous multi-electrode recordings from two brain areas in awake small animals. *J Neurosci Methods* 2007;162:129–38.
- Leutgeb S, Leutgeb JK, Moser MB, Moser EI. Place cells, spatial maps and the population code for memory. *Curr Opin Neurobiol* 2005;15:738–46.
- Lin L, Chen G, Xie K, Zaia KA, Zhang S, Tsien JZ. Large-scale neural ensemble recording in the brains of freely behaving mice. *J Neurosci Methods* 2006;155:28–38.
- Mansuy IM, Bujard H. Tetracycline-regulated gene expression in the brain. *Curr Opin Neurobiol* 2000;10:593–6.
- McHugh TJ, Blum KI, Tsien JZ, Tonegawa S, Wilson MA. Impaired hippocampal representation of space in CA1-specific NMDAR1 knockout mice. *Cell* 1996;87:1339–49.
- McHugh TJ, Jones MW, Quinn JJ, Balthasar N, Coppari R, Elmquist JK, et al. Dentate gyrus NMDA receptors mediate rapid pattern separation in the hippocampal network. *Science* 2007;317:94–9.
- McNaughton BL. Comments in hippocampus symposium panel discussion. In: Siefert W, editor. *Neurobiology of the hippocampus*. New York: Academic Press; 1983. p. 610.
- McNaughton BL, Battaglia FP, Jensen O, Moser EI, Moser MB. Path integration and the neural basis of the 'cognitive map'. *Nat Rev Neurosci* 2006;7:663–78.
- Nakashiba T, Young JZ, McHugh TJ, Buhl DL, Tonegawa S. Transgenic inhibition of synaptic transmission reveals role of CA3 output in hippocampal learning. *Science* 2008;319:1260–4.
- Nakazawa K, Quirk MC, Chitwood RA, Watanabe M, Yeckel MF, Sun LD, et al. Requirement for hippocampal CA3 NMDA receptors in associative memory recall. *Science* 2002;297:211–8.
- Nakazawa K, McHugh TJ, Wilson MA, Tonegawa S. NMDA receptors, place cells and hippocampal spatial memory. *Nat Rev Neurosci* 2004;5:361–72.
- O'Keefe J, Burgess N. Dual phase and rate coding in hippocampal place cells: theoretical significance and relationship to entorhinal grid cells. *Hippocampus* 2005;15:853–66.
- O'Keefe J, Recce ML. Phase relationship between hippocampal place units and the EEG theta rhythm. *Hippocampus* 1993;3:317–30.
- Tsien JZ, Chen DF, Gerber D, Tom C, Mercer EH, Anderson DJ, et al. Subregion- and cell type-restricted gene knockout in mouse brain. *Cell* 1996;87:1317–26.
- Ulanovsky N, Moss CF. Hippocampal cellular and network activity in freely moving echolocating bats. *Nat Neurosci* 2007;10:224–33.
- Wilson MA, McNaughton BL. Dynamics of the hippocampal ensemble code for space [see comments] [published erratum appears in *Science* 1994 Apr 1;264(5155):16]. *Science* 1993;261:1055–8.
- Yamamoto J, Wilson MA. Large-scale chronically implantable precision motorized microdrive array for freely behaving animals. *J Neurophysiol* 2008.